

Field testing of multicomponent DAS sensing

Kevin W. Hall, Kris Innanen and Don C. Lawton

ABSTRACT

We constructed an experimental directional DAS sensor (DDS) at the Containment and Monitoring Institutes Field Research Station (CaMI.FRS) in 2018. The sensor consists of two buried 10x10 m squares of straight and helically wound fibre, with the second square rotated forty-five degrees relative to the first. Three-component geophones were planted on the surface just outside of the corners of the DDS, and four source locations (Vibe Points) were acquired using a 5 m gauge length in the DAS interrogator.

Building on work reported last year, where horizontal components of the geophone data were converted to strain-rate traces and visually compared to fibre strain-rate traces, we use directional strain-rate traces to estimate time-series of strain-rate-tensors for the DDS and surface geophones for the first direct ground-roll arrival across the DDS.

The estimated tensors are almost identical for the straight and helically wound fibre after trace scaling, but the amplitudes of the geophone strain-rate tensors are higher than seen for the fibre results in some cases. We speculate this is because the geophones and the fibre are not co-located.

INTRODUCTION

In this year's CREWES report are a range of papers outlining progress towards new seismic based methods for monitoring injection, both statically and in time-lapse settings. Waveform algorithms and their potential augmentation with data from new sensing technology, e.g., fibreoptics, are currently under development. It seems clear at present that the ability of fibreoptic sensors to support seismic surveys without interrupting production and/or injection, and new acquisition geometries it affords while doing so (e.g., along horizontal and vertical well trajectories), make DAS an extremely valuable data mode to support waveform methods. However, the challenges of DAS data remain, including its highly directional and single-component nature. The possibility exists that, through specific, but still relatively practical, deployment of loops of DAS fibre at certain points in a layout, multiple components of the arriving seismic strain field can be inferred and effectively sensed. This would be a key enabler of waveform methods for monitoring, both in hydrocarbon production monitoring, and in monitoring of CO₂ injection and containment.

Motivated by this, an experimental Directional DAS Sensor (DDS) was buried at the Containment and Monitoring Institutes Field Research Station (CaMI.FRS) in 2018 (Innanen et al., 2019; Hall et al., 2020). The sensor consists of two buried 10x10 m horizontal square loops of fibre, with the second square rotated forty-five degrees relative to the first. Three-component geophones were planted on the surface just outside of the corners of the DDS, oriented to magnetic North (Figure 1). We recorded four Vibe Points (VP) on the DDS in 2008 at four different offsets and two different azimuths. This report

details a method to generate time series strain-rate tensors from the first ground-roll arrivals recorded on the straight and helical fibre in the DDS, as well as on the surface geophones.

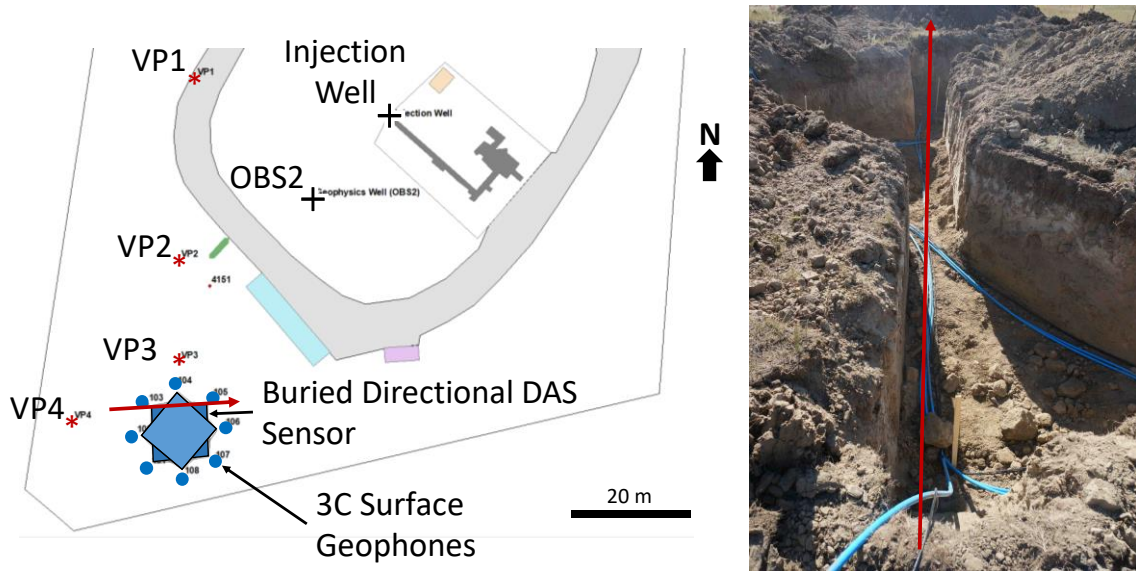


FIG. 1. Directional DAS sensor, surface geophones and vibe point locations (left). Photo of the straight fibre cable (black) and helical fibre cable (blue) looking from station 103 to 105 (red arrows).

METHOD

If it were possible to construct a true "multicomponent strain-rate sensor", it would generate 6 independent traces. At each sample point, the 6 numbers would represent the instantaneous values of the 6 independent components of strain-rate that a seismic wave carries, expressed in some reasonable coordinate system. If we choose to use geographic coordinates, we could use North-South (N), East-West (E), and Depth (D). We would then express the entire response as a $3 \times 3 \times Nt$ cube:

$$e(t) = \begin{bmatrix} e_{EE}(t) & e_{EN}(t) & e_{ED}(t) \\ e_{EN}(t) & e_{NN}(t) & e_{ND}(t) \\ e_{ED}(t) & e_{ND}(t) & e_{DD}(t) \end{bmatrix}. \quad (1)$$

However, the DDS has no coverage in the depth direction, so we are not able to estimate any elements of Equation 1 that contain a 'D' in their name. In fact, we can only solve the reduced problem of finding the 3 independent components of

$$e = \begin{bmatrix} e_{EE} & e_{EN} \\ e_{EN} & e_{NN} \end{bmatrix}. \quad (2)$$

So, our goal is to build a "machine" that outputs 3 traces, whose sample points represent $e_{NN}(t)$, $e_{EN}(t)$, and $e_{EE}(t)$. This would then be a $3 \times 3 \times Nt$ cube, of the form

$$e(t) = \begin{bmatrix} e_{EE}(t) & e_{EN}(t) \\ e_{EN}(t) & e_{NN}(t) \end{bmatrix}. \quad (3)$$

Data preparation

We can build this from the response of the DDS, if we have the following: (1) One directional strain-rate trace derived from each side of each square in the DDS, with samples representing the strain-rate along that direction in as isolated a way as possible, and (2) corrections applied to each trace for moveout across the shape of the DDS. Initially, we intend to flatten on a horizon pick, so that each sample in any given trace is sensing the same part of the arriving wave at the same time, mimicking a point sensor. The output of the above will comprise 8 traces. One sample point across these 8 traces will represent strain-rate measured in 4 independent directions in the EW-NS plane. We can arrange these in a matrix with 8 columns and rows for each time sample

$$e_i(t) = [e_1(t) \quad e_2(t) \quad e_3(t) \quad e_4(t) \quad e_5(t) \quad e_6(t) \quad e_7(t) \quad e_8(t)], \quad (4)$$

where i represents DDS directions 1 through 8.

None of the 8 directions line up precisely with UTM grid north or east, but from the GPS survey of the DDS before it was buried, we can determine the azimuths of the sides of the DDS relative to grid north. We can also populate Equation 4 with directional strain-rate traces calculated from the surface 3C geophones using the method shown by Hall et al. (2020). Note that if we desire time-series of strain, we just integrate our strain-rate traces with respect to time.

Tensor estimation

With the DDS response processed to approximate that of a point sensor, the raw strain-rate (or strain) measurements can be transformed into a set of geometrically self-consistent tensor components in the field coordinate system. Let us specify the field system precisely, by letting the N axis be the vertical axis and the E axis be the horizontal axis in a 2D Cartesian grid. In this system the northing and easting unit vectors are

$$\hat{t}_N = \begin{bmatrix} 0 \\ 1 \end{bmatrix} \text{ and } \hat{t}_E = \begin{bmatrix} 1 \\ 0 \end{bmatrix}. \quad (5)$$

Each of the fibre line segments in (11, 12, 13, 14, 21, 22, 23, 24; Figure 2) have directional unit vectors as well, and there are 8 of these:

$$\hat{t}_1 = \begin{bmatrix} t_1^1 \\ t_1^2 \end{bmatrix}, \hat{t}_2 = \begin{bmatrix} t_2^1 \\ t_2^2 \end{bmatrix}, \dots, \hat{t}_8 = \begin{bmatrix} t_8^1 \\ t_8^2 \end{bmatrix}. \quad (6)$$

Determining all of these unit vectors from the geographic information in the previous section, we can then form a linear system relating the actual strain (or strain rate) arriving at the sensor at a particular instant, in the field system, to those being sensed in the 8 fibre loop directions:

$$\begin{bmatrix} e_1 \\ \vdots \\ e_8 \end{bmatrix} = L \begin{bmatrix} e_{EE} \\ e_{EN} \\ e_{NN} \end{bmatrix}, \quad (7)$$

where

$$L = \begin{bmatrix} \lambda_{EE}^1 & 2\lambda_{EN}^1 & \lambda_{NN}^1 \\ \vdots & \vdots & \vdots \\ \lambda_{EE}^8 & 2\lambda_{EN}^8 & \lambda_{NN}^8 \end{bmatrix} \quad (8)$$

and where

$$\lambda_{AB}^i = (\hat{t}_i \cdot \hat{t}_A)(\hat{t}_i \cdot \hat{t}_B), \quad (9)$$

with A, B ranging over E, N. Given variable directional coverage (which the DDS provides), this is an overdetermined system which can be solved for the 3 independent components of strain:

$$\begin{bmatrix} e_{EE} \\ e_{EN} \\ e_{NN} \end{bmatrix} = (L^T L + \alpha I)^{-1} L^T \begin{bmatrix} e_1 \\ \vdots \\ e_8 \end{bmatrix}. \quad (10)$$

Fibre geometry

In order to isolate fibre traces along each line segment of the DDS and create line segment gathers (LSG), we build a model of the fibre path through the DDS and interpolate trace locations along the fibre path given the interrogator trace spacing. The geometry model used last year consisted of straight line segments joining the GPS locations of the corners of the squares, and did not take into account the length of fibre in the transition between the two squares, the fact that the corners were rounded so as not to introduce kinks in the fibre cables in the field, or honor GPS data that was acquired at the approximate locations where cables from the two squares cross-over.

Figure 2 shows the updated DDS geometry model that was constructed for this report. The slopes of the line segments between the corner GPS locations (last year's model) were used as a constraint. The lines were then allowed to move equal distances perpendicularly from their initial locations in a least-squares regression, allowing each square to expand in size in order to find line locations that best-fit all eight cable cross-over locations. The outward shift that best fits the cross-over GPS locations is 0.3 m. Then, we ran a second least-squares regression to find the radius of circles tangent to the shifted lines, such that the circumference of the circle best-fits our corner GPS locations. The best-fit radius for the circles is 0.9 m, which is reasonably close to our field observation of approximately one metre.

The coordinates were then replicated and assembled to create a fibre path (gray squares with rounded corners; Figure 2) that begins halfway along the circle closest to station 104, travels around square 1 (stations 104,106,108,102,104) twice, transitions from station 104 through a cross-over point to station 105 (purple arrow); Figure 2), and finishes by travelling around square 2 (stations 105, 107, 101, 103, 105) twice before exiting the DDS at station 105. Given the straight fibre (1.025 m) or corrected helical fibre trace spacing (0.907 m) for the 2018 survey (Hall et. al, 2019), we can interpolate coordinates for trace

locations along the fibre path (black, red, and blue dots; Figure 2). For the remainder of this report, straight fibre traverses squares 1 and 2 and helical fibre traverses the same squares but renumbered to 4 and 5.

Geophone geometry

Hall et al. (2020) calculated directional strain-rate by rotating the horizontal components of a pair of geophones so one of the rotated components was parallel to the side of a square, subtracted the resulting traces and divided by the distance between them. The output trace was then located at the halfway point along a straight line between geophone stations. This year, we have taken the additional step of projecting the strain-rate trace locations onto the closest line segment of the fibre loop model (black diamonds; Figure 2). We are now able to calculate the distance from the beginning of the fibre path to each geophone strain-rate trace for an arbitrary trace spacing. Note that each strain-rate trace appears in the fibre path four times (2x square 1 followed by 2x square 2).

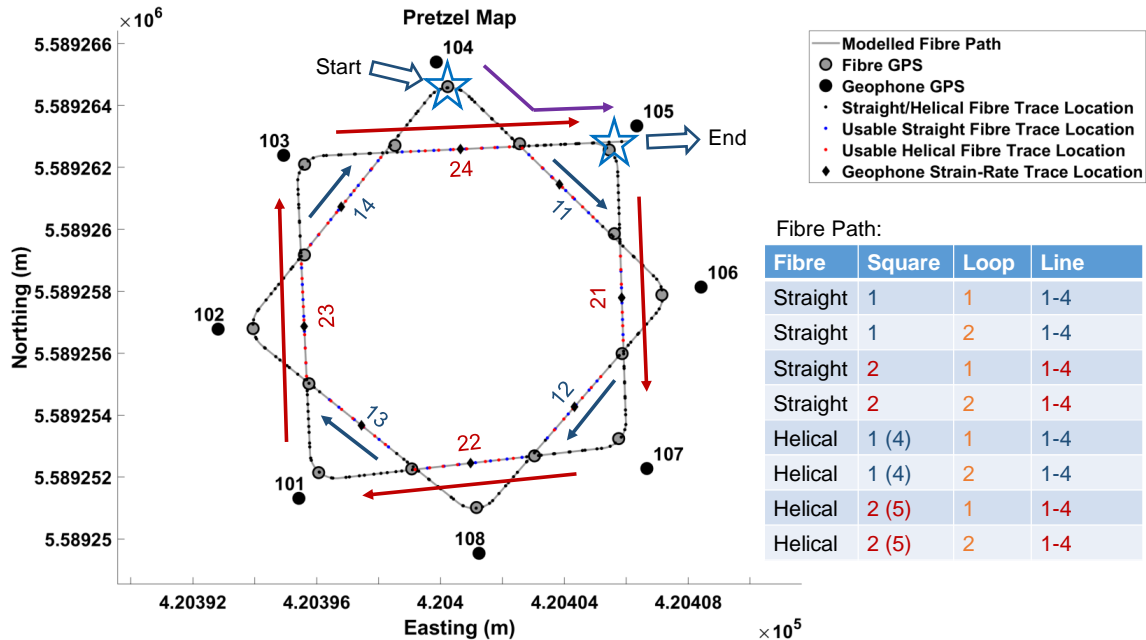


FIG. 2. Detail of the 2020 directional DAS sensor (DDS) geometry model. Note that the straight and helical fibre enter the ground near station 103, but we are neglecting the fiber distance from 103-104 in our model. Arrows show the direction of increasing distance from the interrogator along the fibre path. Numbers in the center of the map are DDS (Square)*10+Line. Red and blue dots along the fibre path are straight and helical fibre trace locations where the data has no contributions from the corners or other sides of the squares.

Data expectations

It is difficult to interpret events on source gathers that only have a 10 m window of traces, so it is helpful to examine data from other surveys in the same area. Figure 3 shows the inline component of a 3C surface geophone source gather from a 2017 survey described by Hall et al., (2018) with direct arrival, air blast and ground roll highlighted. Ground roll is dispersive, meaning that different frequencies travel at different velocities, and is typically aliased (Figure 4). The fastest ground-roll velocity is very similar to the air blast

velocity. These figures show that we should expect prominent ground-roll on our DDS data, mixed with higher frequency direct arrivals, and air blast on the geophone data.

In terms of our tensor estimation plan for this data, it is clear that we will not be able to use the direct arrivals due to air-blast contamination, and the DDS cannot easily be considered to be a point receiver for ground-roll unless we focus on a small part of the ground-roll, such as just the peak at v_1 in Figure 3. The air-blast and direct arrivals can be attenuated by applying a bandpass filter to enhance the ground-roll.

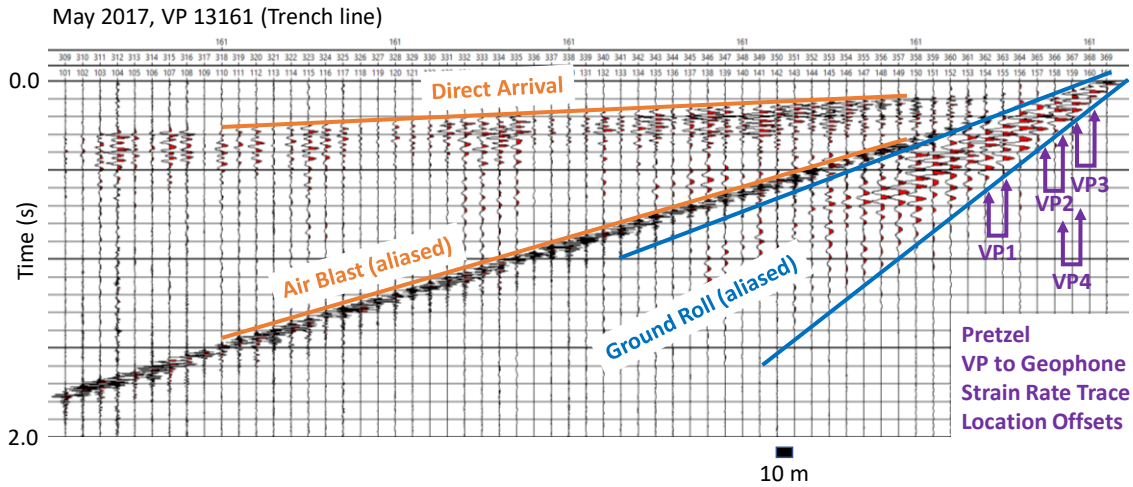


FIG. 3. Inline component of the closest source gather to the DDS, VP 13161, May 2017, Trench Line. Equivalent offsets from DDS VPs 1-4 to the DDS are highlighted with purple arrows. Data are displayed with no filters.

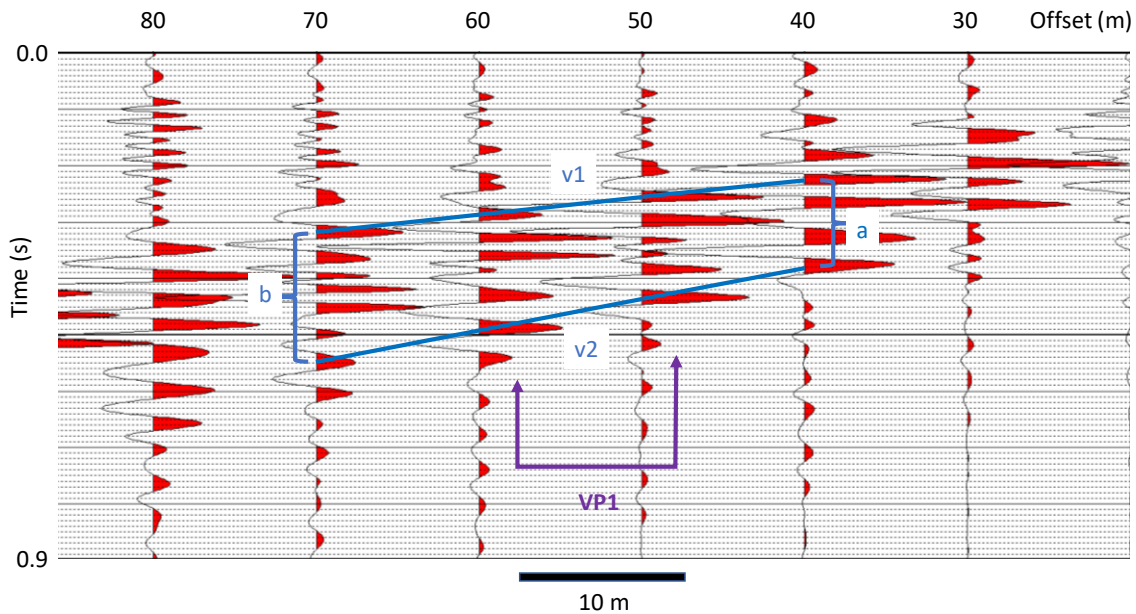


FIG. 4. Detail of Figure 3. Over a 30 m distance, the data vary from 2 peaks between the blue lines at (a) to 5 peaks at (b). Data are displayed with no filters.

Data preparation

In order to estimate strain-tensor time series, we need to extract traces from each line segment of each square of the DDS to form line segment gathers (LSG) that can be aligned and vertically stacked. These traces should not contain any data contributions from the corners or the sides of the DDS due to the gauge length (5 m) used in the interrogator.

Figure 5 shows an example of straight fibre data from the DDS for VP1, where the trace location corresponding to the start of our fibre model has been interpreted, and coordinates and dead trace flags obtained from the fibre model have been imported to the trace headers. The middle and right-hand sides of the figure highlight the traces to be extracted for line segment gathers. Direct arrivals and air blast can be seen starting at about 200ms, with high-amplitude low-frequency ground-roll arriving at about 300 ms. The ground-roll shows significant moveout over 5 m of horizontal distance (Figure 5; right).

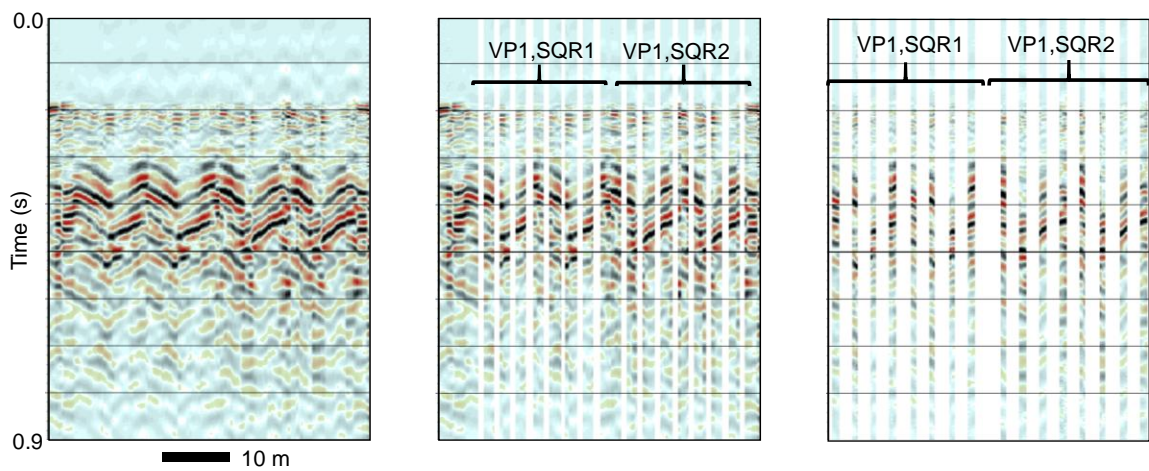


FIG. 5. Strain rate data for VP 1, Squares 1 and 2 (left), with desired traces for LSG removed (middle) and kept (right).

Figure 6 shows straight and helical strain-rate line segment gathers (cf. Figure 5, right), after alignment using cross-correlations vertical stack and a 10-30 Hz bandpass filter. The output traces are shifted to the average arrival time for each LSG. The vertically stacked fibre data is interleaved with directional strain-rate traces calculated from the surface geophones such that odd numbered traces are fibre and even numbered traces are geophone. The left half of each VP is straight fibre and geophones, and the right half is helical fibre and repeated geophone traces. We have combined all three data types to ease the task of identifying the same peak on all data sets. The trough before the first identifiable ground roll peak have been picked as a horizon (TREF1).

Figure 7 shows the same data after flattening TREF1 to the horizon pick time for the first fibre trace in each source gather, and horizon picks for the next trough (TREF2). TREF2 does not line up horizontally. We are attributing this to the fact that the same ground roll peak on an adjacent trace will be lower frequency as well as being recorded later with increasing offset. In order to make the DDS approximate a point-receiver, we keep TREF1

aligned and linearly stretch each trace in each source gather until TREF2 best matches that of the first fibre trace in the gather (Figure 8).

There are 5 dead traces in Figure 8 because our trace stretching algorithm failed for currently unknown reasons. However, we still have far more directional strain-rate traces than unknowns, so we can use the traces shown in Figure 8 to populate Equation 4 and carry on with estimating the strain-rate tensors.

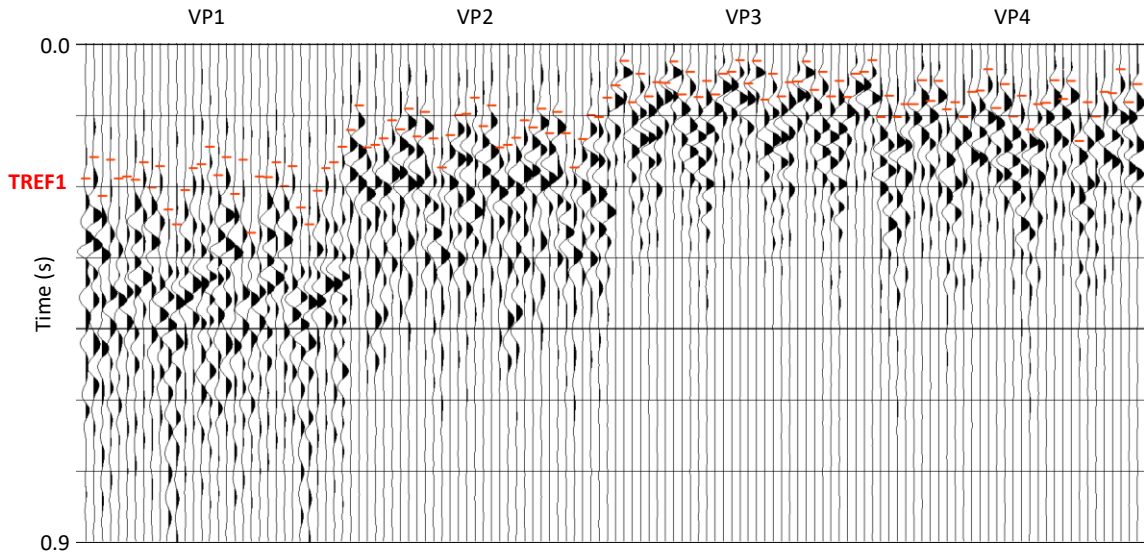


FIG. 6. Vertically stacked straight and helical fibre line segment gathers interleaved with directional strain-rate traces calculated from geophone data.

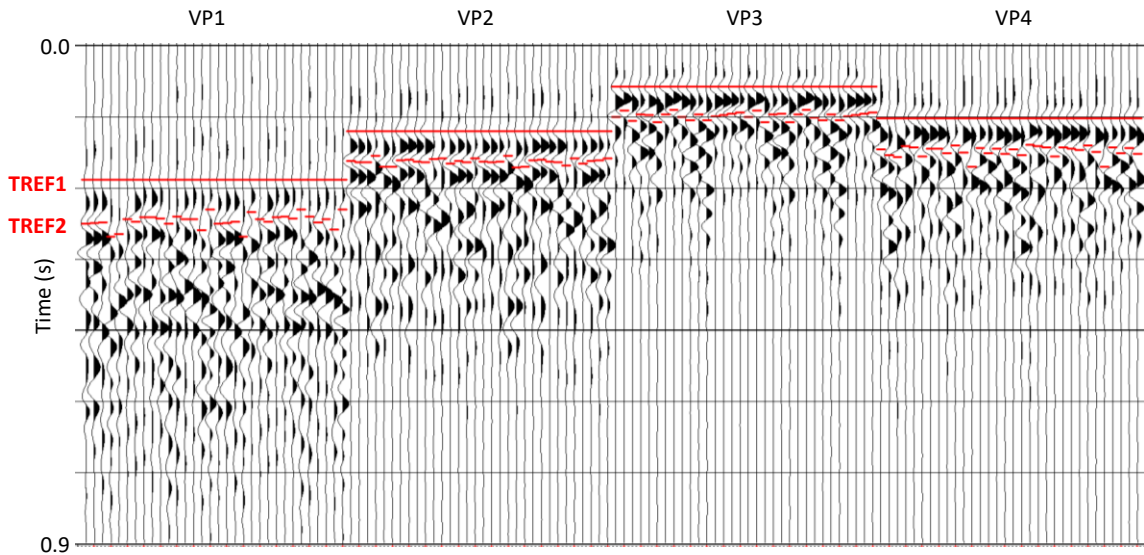


FIG. 7. Vertically stacked straight and helical fibre line segment gathers interleaved with directional strain-rate traces calculated from geophone data, aligned on trough before first ground-roll peak.

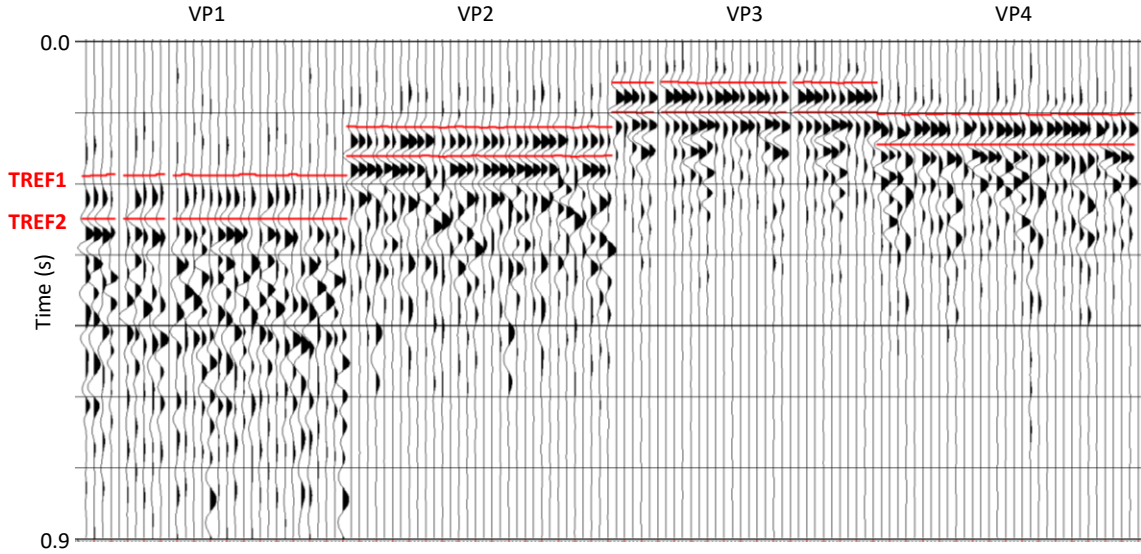


FIG. 8 Vertically stacked straight and helical fibre line segment gathers interleaved with directional strain-rate traces calculated from geophone data, aligned on trough before first ground-roll peak and stretched to align trough after first ground-roll peak.

RESULTS

Our expectation for VP1, VP2 and VP3 is that e_{EN} should have the most energy and e_{EE} should have the least. In contrast VP4 should have the most energy on e_{EE} and the least on e_{EN} . Figure 9 shows strain-rate tensors e_{EE} , e_{EN} and e_{NN} estimated from traces shown in Figure 8 using Equation 10 for a time window defined by TREF1 and TREF2 ± 25 samples. Gathers are individually scaled for display. The straight and helical fibre tensors plot practically on top of each other, and the geophone results are very similar although with higher relative amplitudes for VP2 (e_{EE} , e_{EN}) and VP4 (e_{EN}). The results match our expectations prior to doing the calculations. To the best of our knowledge, Figure 9, represents the first strain-rate-tensor estimation result from a directional DAS sensor.

DISCUSSION AND FUTURE WORK

The prototype multicomponent DAS sensor was designed with a 5-10m gauge length in mind, and given this limitation we view these results as being positive, and strongly indicative of the possibilities of the approach. However, the large size of the loop required in such a design, and the pre-processing it makes necessary (in order to create the dataset which would have been measured if the same parts of the seismic wave-front arrived at all points on the loop simultaneously), has led to fairly serious uncertainties. We regard the design and burial of a next generation of sensor loop, in which the lengths are on the order of 2m, and interrogation of this sensor with gauge lengths on the order of 1m, to be a critical next step.

Our present analysis is also suggestive that any further pre-processing for validation purposes would also be made significantly simpler if there were regions of the data dominated by body wave energy; more distant vibroseis points are indicated. Both the use of smaller gauge lengths and more distant vibroseis points will tend to exacerbate SNR issues in

the data. For validation purposes this can probably be overcome with a lengthening of the vibe sweep, and with source repetition.

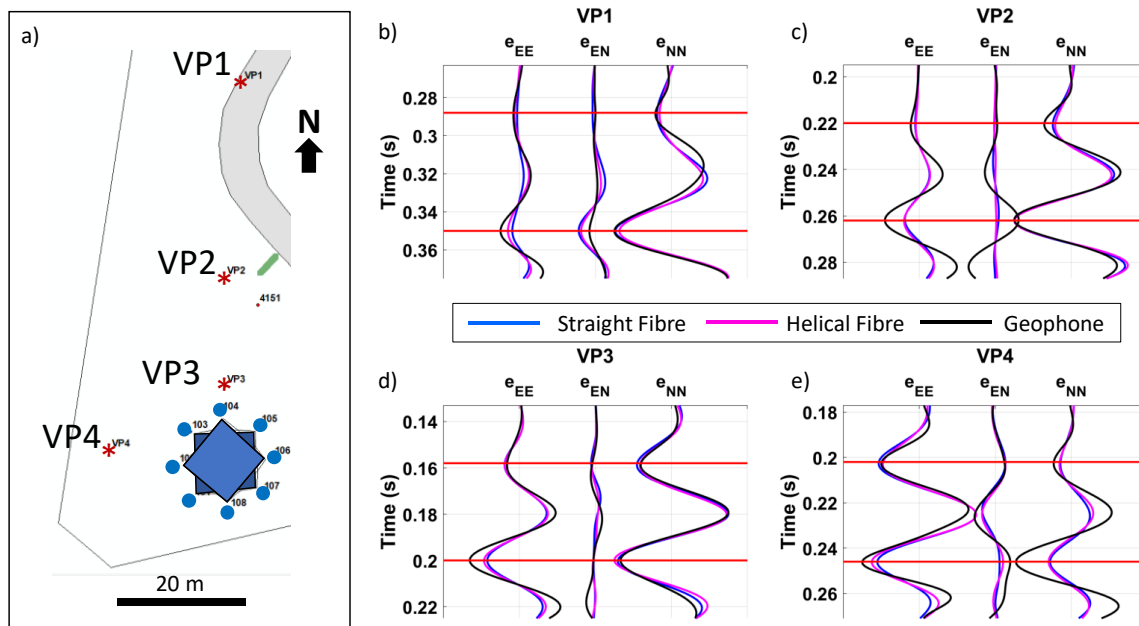


FIG. 9. Map showing four Vibe points, DDS, and geophone locations (a), and strain-rate tensors estimated for the first identifiable ground-roll peak for VP1 (b), VP2 (c), VP3 (d), and VP4 (e).

ACKNOWLEDGEMENTS

The sponsors of CREWES are gratefully thanked for continued support. This work was funded by CREWES industrial sponsors, NSERC (Natural Science and Engineering Research Council of Canada) through the grants CRDPJ 461179-13 and CRDPJ 543578-19, and in part by an NSERC-DG. We would also like to thank Halliburton for the field acquisition, Schlumberger for the use of donated Vista software, and all CREWES sponsors and CaMIFRS JPI subscribers for their continued support.

REFERENCES

- Hall, K. W., Lawton, D. C., Daley, T., Freifeld, B., Marchesini, P., and Cook, P., 2018, Effect of source effort and source distance on optical fibre data at CaMIFRS, Newell County, Alberta: *88th Annual International Meeting, SEG, Expanded Abstracts*.
- Hall, K. W., Innanen, K. A. H., and Lawton, D. C., 2020, Comparison of multi-component seismic data to fibre-optic (DAS) data: *90th Annual International Meeting, SEG, Expanded Abstracts*.
- Innanen, K. A. H., Lawton, D. C., Hall, K. W., Bertram, K. L., Bertram, M. B., and Bland, H. C., 2019, Design and deployment of a prototype multicomponent Distributed Acoustic Sensing loop array: *89th Annual International Meeting, SEG, Expanded Abstracts*.